Scripta Materialia 157 (2018) 72–75

Contents lists available at ScienceDirect

Scripta Materialia

journal homepage: www.elsevier.com/locate/scriptamat

Regular article

3D characterization of partially recrystallized Al using high resolution diffraction contrast tomography

Jun Sun [a,b], Tianbo Yu [a], Chaoling Xu [c], Wolfgang Ludwig [d,e], Yubin Zhang [a,*]

[a] Department of Mechanical Engineering, Technical University of Denmark, 2800 Kgs. Lyngby, Denmark
[b] Xnovo Technology, 4600 Køge, Denmark
[c] Department of Management and Engineering, Linköping University, SE-58183 Linkoping, Sweden
[d] ESRF, 6 rue Jules Horowitz, Grenoble 38043, France
[e] University of Lyon, MATEIS, INSA-Lyon, UMR 5510 CNRS, 7 Avenue Jean Capelle, Villeurbanne 69621, France

ARTICLE INFO

Article history:
Received 29 June 2018
Received in revised form 31 July 2018
Accepted 1 August 2018
Available online xxxx

Keywords:
Recrystallization
3D reconstruction
Schwartz-Saltykov analysis
Electron backscattering diffraction (EBSD)
Aluminium

ABSTRACT

Synchrotron diffraction contrast tomography (DCT) is for the first time used to characterize recrystallized grains in partially recrystallized Al. The positions, orientations and 3D shapes of >900 recrystallized grains are reconstructed within a gauge volume. The results are compared with those obtained using electron backscattered diffraction based on a statistical analysis. It is found that recrystallized grains with size larger than 10 μm, corresponding to ~98% of the total recrystallized volume of the sample, are well characterized by DCT. The advantages of DCT for recrystallization studies and new possibilities with DCT on new generation synchrotron sources are discussed.

During recrystallization of deformed materials, nearly defect-free nuclei/grains form and grow at the expense of the surrounding deformed matrix. Recent 3D results obtained using serial sectioning have shown that the distribution of nuclei/recrystallized grains is non-uniform, and depends strongly on the local deformation microstructure [1–4]. Although both deformed matrix and nuclei/recrystallized grains can be characterized with these techniques, only limited volume or limited spatial resolution can be obtained when the sectioning is done with focused ion beam [1] or mechanical polishing [2–4], respectively. More importantly, the destructive nature of the techniques prohibits the possibility of dynamic studies to follow the recrystallization process, which is essential for a better understanding of the heterogeneities of recrystallization.

During the last 15–20 years, several non-destructive 3D characterization techniques have been invented and implemented using synchrotron X-rays, including 3D X-ray diffraction (3DXRD) [5–8], diffraction contrast tomography (DCT) [9,10], Bragg coherent diffraction imaging [11,12] and 3D X-ray Laue microdiffraction [13,14]. Among these techniques, DCT allows fast 3D reconstruction of grains in fully recrystallized samples [15,16]. Although the nuclei/grains in partially recrystallized samples are also in the recrystallized state (i.e. with very low densities of interior defects), the nuclei/grains are relatively small compared to those in fully recrystallized samples. At the same time, parts of the microstructure consist of deformed grains with significant orientation variations and strain gradients. Some of the nuclei/grains may have orientations similar to the neighboring deformed grains, from which they originate. All these factors make reconstruction of the recrystallized grain very challenging [10]. To what extend DCT can be used to characterize partially recrystallized samples is therefore still an open question.

In the present paper, we will for the first time explore the applicability of DCT for recrystallization characterization. A partially recrystallized Al sample will be used as a model material. To validate the DCT results, they will be compared with those obtained based on conventional characterization using electron backscattered diffraction (EBSD). Statistical analysis will be performed to link the 2D EBSD and the 3D DCT results and ease the interpretation of the results.

Commercial purity aluminium, Al1050, was used for the present study. The starting material had a fully recrystallized microstructure with an average grain size of ~50 μm. The material was then cold rolled to 50% reduction in thickness, followed by annealing at 325 °C for 0.5 h to obtain a partially recrystallized microstructure. For the synchrotron DCT measurement, pillar samples with cross-section of ~420 × 420 μm^2 were cut out using electrical discharge machining. The DCT measurement was conducted at beamline ID11 at the European Synchrotron Radiation Facility (ESRF). The X-ray energy was 37 keV. The direct X-ray beam was constrained by two sets of vertical and horizontal slits to 240 × 420 μm^2. Transfocators with beryllium lenses were used to focus the

* Corresponding author at: Technical University of Denmark, Produktionstorvet, Building 425, room 214, 2800 Kgs. Lyngby, Denmark.
E-mail address: yubz@mek.dtu.dk (Y. Zhang).

https://doi.org/10.1016/j.scriptamat.2018.08.001
1359-6462/

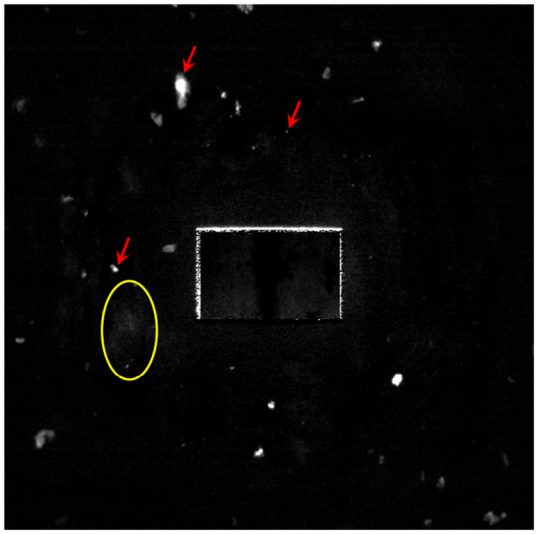

Fig. 1. A typical near-field diffraction image of the partially recrystallized Al sample, recorded using a near-field detector with 2048 × 2048 pixels (pixel size of 0.77 μm). The red arrows mark examples of diffraction spots originating from recrystallized grains, while the yellow ellipse marks diffraction from a deformed grain. The rectangle region in the middle is from the direct X-ray beam. (For interpretation of the references to color in this figure legend, the reader is referred to the web version of this article.)

beam. A uniform beam was obtained within the defined gauge. The sample was mounted on an ω rotation stage with the sample rolling direction (RD) parallel to the vertical rotation axis. A full 360° scan was performed with angular integration steps of 0.1° and an exposure time of 2 s for each projection. Both the diffracted and the transmitted beam were recorded using a near-field detector (comprising a transparent luminescent screen, light optically coupled to a CCD) with 2048 × 2048 pixels positioned normal to the incident beam at a sample-to-detector distance of 3 mm. To improve the spatial resolution, an eyepiece was used to magnify the diffraction images. The effective pixel size of the detector system was 0.77 μm. The detailed information about the DCT setup can be found in [9,10].

A typical diffraction image is shown in Fig. 1. Most of the diffraction spots, e.g. those marked by the red arrows, are sharp and well-defined, appearing typically at 1–2 consecutive angular steps. These diffraction spots originate from recrystallized grains. Only few blurry, large and weak diffraction spots, as the one marked by the yellow ellipse, are visible and appear typically over a large number of angular steps. These originate from the deformed matrix.

Table 1
Microstructural parameters for recrystallized grains calculated based on DCT and EBSD data. V_V, D_{ESD}, N_V and N_{total} are volume fraction, average grain size, number of grains per unit volume and total grain number, respectively. For EBSD data, the D_{ESD} was calculated based on the statistical analysis.

	V_v	D_{ESD} (μm)	N_V (10^{-5} μm^{-3})	N_{total}
DCT	24%	18.4	2.7	929
EBSD	28 ± 4%	14.6	4.1	469

The diffraction images were analyzed with the DCT software (http://sourceforge.net/projects/dct) available at the beamline. A recently developed algorithm allowing 6D reconstruction (3D for position + 3D for orientation) [17,18] is used to reconstruct the grain shapes. In total 929 recrystallized grains are found within the gauge volume. The 3D volume is shown in Fig. 2a. The recrystallized grains are typically not spherical but elongated along the RD and the transverse direction (TD). Also the recrystallized grains are not randomly distributed, but clustered in bands parallel to the RD and TD. For clear visualization, a typical 2D section is shown in Fig. 2b. The volume fraction, V_V, of the recrystallized grains is about 24% and the average grain size (defined as equivalent spherical diameter (ESD)) is about 18 μm. The number of grains per unit volume, N_V, (determined by N_{total}/V, where V is the gauge volume) is about 2.7 × 10^{-5} μm^{-3} (see Table 1).

To verify the 3D results, the microstructure of the sample was characterized using a Zeiss Supra 35 field emission gun scanning electron microscope equipped with a Channel 5 EBSD system. EBSD measurements were conducted on the longitudinal section (defined by the RD and normal direction (ND)) using a scanning step size of 0.5 μm, covering two areas of ~6.7 × 10^5 μm^2.

An example of the EBSD maps is shown in Fig. 3a. The recrystallized grains are selected from the EBSD maps using the following criteria: i) grain size (equivalent circular diameter, ECD), larger than 3 μm, ii) surrounded at least partly by high angle boundaries to the deformed matrix, iii) the internal misorientation angle is <1°. Fig. 3b shows the recrystallized grains only. Similar to the 3D results, clusters of recrystallized grains are seen in bands parallel to the RD. In total, 469

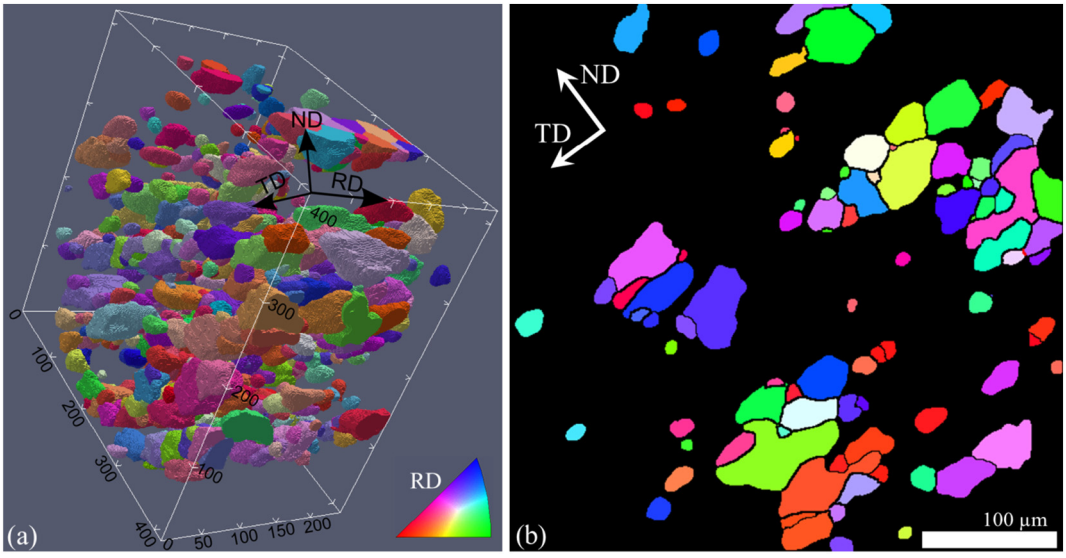

Fig. 2. 3D reconstruction of recrystallized grains measured by DCT. (a) The 3D volume of 240 × 420 × 420 μm^3; (b) a 2D section. The colors in both (a) and (b) represent the crystallographic orientation along RD (see the inset in (a)). In (b) thin and thick black lines represent boundaries with misorientation >2° and >15°, respectively. The voxel/pixel size is 0.77 μm. (For interpretation of the references to color in this figure legend, the reader is referred to the web version of this article.)

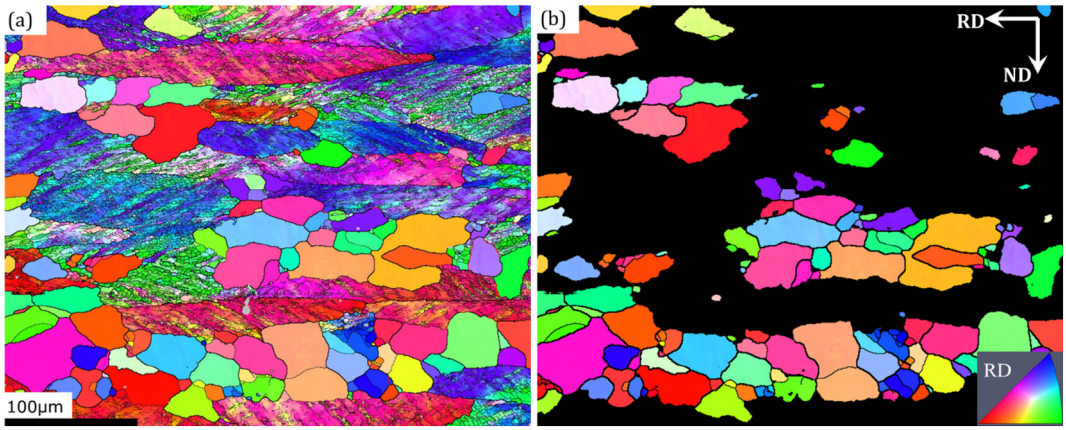

Fig. 3. Example of microstructure of the partially recrystallized Al sample: (a) full map, (b) recrystallized grains. The colors used in the EBSD maps correspond to the crystallographic orientations along sample RD (see the inset in (b)). Thin and thick black lines represent boundaries with misorientation >2° and >15°, respectively. The pixel size of the EBSD map is 0.5 μm. (For interpretation of the references to color in this figure legend, the reader is referred to the web version of this article.)

recrystallized grains are found. The V_V determined based on EBSD maps is slightly higher than that of the 3D result.

It should be noted that on the EBSD maps not all grains are sectioned through their maximum diameter; many grains appear smaller than they actually are, and large grains have a higher chance to be sectioned than small grains. A statistical analysis using stereology is required to link the 2D EBSD and 3D DCT data. In the present paper, the Schwartz-Saltykov (SS) method, which is a standard way to calculate 3D grain size (D_{ESD}) distribution based on the 2D size (D_{ECD}) distribution [19], is performed to calculate the N_V and the average grain size (see the supplementary materials).

The results show that the N_V determined from SS analysis is ~30% higher than that from DCT data (see Table 1). In other words, ~30% of the recrystallized grains are not seen in the DCT data set. To further understand the missing grains, the distributions of N_V calculated from DCT and EBSD data are compared (see Fig. 4). It is evident that the two distributions agree well to each other for the size range larger than 10 μm, whereas DCT significantly underestimated the fraction of the small grains (<10 μm). This comparison suggests that the low N_V of the DCT data is primarily attributed to the small grains, which have been poorly indexed by DCT. As a result, the average grain size determined based on the DCT data is larger than that from the SS analysis, while the volume fraction of the recrystallized grains measured from DCT data is slightly smaller than that from EBSD data (see Table 1).

The reason for the poor indexing of the small recrystallized grains is that the small grains (especially in volumes) produce weak diffraction spots, which are difficult to distinguish from the background noise and the diffused diffraction signal from deformation matrix. As the intensities of diffraction spots from hkl families with high numbers are much weaker than those with low numbers, identification of high numbered hkl diffraction spots for even medium size grains (in the range 7–10 μm) is a challenge. As a result, only a limited number of diffraction spots from low numbered hkl families can be segmented properly, which is insufficient for indexing and reconstructing the grains.

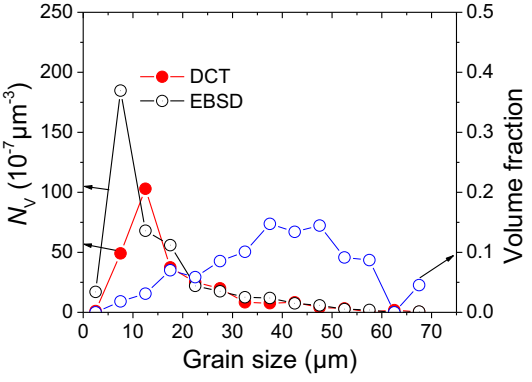

Fig. 4. Distributions of grain size (D_{ESD}) and volume fraction of recrystallized grains determined based on EBSD and DCT data. The volume fraction is calculated based on the distribution of N_V from the EBSD data using SS method.

Despite the large number of the small recrystallized grains which are not indexed by DCT, the volume fraction of those small grains is only <2% of the total volume fraction of the recrystallized grains (see Fig. 4). As recrystallization proceeds and the nuclei/grains grow to large sizes and thus can be properly reconstructed, this situation can be further remedied.

Compared with other 3D characterization techniques, such as 3DXRD [20–23] and X-ray Laue microdiffraction [24,25], DCT has several advantages for recrystallization studies. i) A large number of grains can be characterized simultaneously, allowing a statistically-sound analysis, e.g. the 3D recrystallization kinetics. ii) DCT provides fast measurements of reasonably large volumes (e.g. 400 × 400 × 300 μm^3). A typical DCT scan takes about 2 h. With the upcoming synchrotron upgrade, the X-ray intensity can be improved by a factor of 40–100 [26]. With that implemented, both the spatial resolution (in term of the minimum detectable grain size) and the temporal resolution can be improved significantly. In combination with in-situ annealing, dynamic studies of recrystallization can be performed in the near future.

Acknowledgements

YZ thanks Prof. D. Juul Jensen for the useful comments during the preparation of the manuscript. This work is partly funded by the Innovation Fund Denmark (IFD) (case number: 5190-00044B). The instrument center Danscatt is acknowledged for travel refund (7055-00005B). JS and YZ thank Mr. Lars Lorentzen at DTU Wind Energy for the help with sample preparation.

Appendix A. Supplementary data

Supplementary data to this article can be found online at https://doi.org/10.1016/j.scriptamat.2018.08.001.

References

[1] W. Xu, M.Z. Quadir, M. Ferry, Metall. Mater. Trans. A Phys. Metall. Mater. Sci. 40 (2009) 1547–1556.
[2] G.H. Fan, Y.B. Zhang, J.H. Driver, D. Juul Jensen, Scr. Mater. 72–73 (2014) 9–12.
[3] Y. Zhang, D. Juul Jensen, Y. Zhang, F. Lin, Z. Zhang, Q. Liu, Scr. Mater. 67 (2012) 320–323.

[4] Z. Sükösd, K. Hannesson, G. Wu, D. Juul Jensen, 3rd Int. Conf. Recryst. Grain Growth, ReX GG III 558–559 (2007) 345–350.
[5] H.F. Poulsen, W. Ludwig, E.M. Lauridsen, S. Schmidt, W. Pantleon, U. Olsen, J. Oddershede, P. Reischig, A. Lyckegaard, J. Wright, G. Vaughan, 31st Risø Int. Symp. Mater. Sci (2011) 101–119.
[6] H.F. Poulsen, J. Appl. Crystallogr. 45 (2012) 1084–1097.
[7] D. Juul Jensen, H.F. Poulsen, Mater. Charact. 72 (2012) 1–7.
[8] S. Schmidt, S.F. Nielsen, C. Gundlach, L. Margulies, X. Huang, D. Juul Jensen, Science 305 (2004) 229–232.
[9] W. Ludwig, P. Reischig, A. King, M. Herbig, E.M. Lauridsen, G. Johnson, T.J. Marrow, J.Y. Buffière, Rev. Sci. Instrum. 80 (2009) 033905.
[10] P. Reischig, A. King, L. Nervo, N. Viganó, Y. Guilhem, W.J. Palenstijn, K.J. Batenburg, M. Preuss, W. Ludwig, J. Appl. Crystallogr. 46 (2013) 297–311.
[11] T.W. Cornelius, O. Thomas, Prog. Mater. Sci. 94 (2018) 384–434.
[12] A. Yau, W. Cha, M. Kanan, G.B. Stephenson, A. Ulvestad, Science 356 (2017) 739–742.
[13] B. Larson, W. Yang, G. Ice, J. Budai, J. Tischler, Nature 415 (2002) 887–890.
[14] B.C. Larson, L.E. Levine, J. Appl. Crystallogr. 46 (2013) 153–164.
[15] A. King, G. Johnson, D. Engelberg, W. Ludwig, J. Marrow, Science 321 (2008) 382–385.
[16] J. Zhang, Y. Zhang, W. Ludwig, D. Rowenhorst, P.W. Voohees, H.F. Poulsen, Acta Mater. 156 (2018) 76–85.
[17] N. Viganò, W. Ludwig, K.J. Batenburg, J. Appl. Crystallogr. 47 (2014) 1826–1840.
[18] N. Viganò, A. Tanguy, S. Hallais, A. Dimanov, M. Bornert, K.J. Batenburg, W. Ludwig, Sci. Rep. (2016) 20618.
[19] E.E. Underwood, Quantitative Stereology, Addison-Wesley, 1970.
[20] F.X. Lin, Y.B. Zhang, W. Pantleon, D. Juul Jensen, Philos. Mag. 95 (2015) 2427–2449.
[21] S. Storm, D. Juul Jensen, Scr. Mater. 60 (2009) 477–480.
[22] S.S. West, S. Schmidt, H.O. Sørensen, G. Winther, H.F. Poulsen, L. Margulies, C. Gundlach, D. Juul Jensen, Scr. Mater. 61 (2009) 875–878.
[23] S. Van Boxel, S. Schmidt, W. Ludwig, Y.B. Zhang, D. Juul Jensen, W. Pantleon, Mater. Trans. 55 (2014) 128–136.
[24] Y.B. Zhang, J.D. Budai, J.Z. Tischler, W. Liu, R. Xu, E.R. Homer, A. Godfrey, D. Juul Jensen, Sci. Rep. 7 (2017) 4423.
[25] C. Xu, Y. Zhang, A. Godfrey, G. Wu, W. Liu, J.Z. Tischler, Q. Liu, D. Juul Jensen, Sci. Rep. 7 (2017) 42508.
[26] ESRF upgrade programme phase II (2015–2019) white paper, 2015.